ARCCB-TR-92014

A NOTE ON THE BLAST SIGNATURE OF A CANNON

G.C. CAROFANO

MARCH 1992

US ARMY ARMAMENT RESEARCH,
DEVELOPMENT AND ENGINEERING CENTER
CLOSE COMBAT ARMAMENTS CENTER
BENÉT LABORATORIES
WATERVLIET, N.Y. 12189-4050

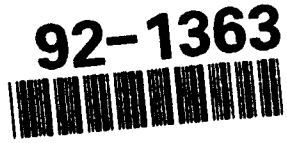

DISCLAIMER

The findings in this report are not to be construed as an official Department of the Army position unless so designated by other authorized documents.

The use of trade name(s) and/or manufacturer(s) does not constitute an official indorsement or approval.

DESTRUCTION NOTICE

For classified documents, follow the procedures in DoD 5200.22-M, Industrial Security Manual, Section II-19 or DoD 5200.1-R, Information Security Program Regulation, Chapter IX.

For unclassified, limited documents, destroy by any method that will prevent disclosure of contents or reconstruction of the document.

For unclassified, unlimited documents, destroy when the report is no longer needed. Do not return it to the originator.

REPORT DOCUMENTATION PAGE

Form Approved
OMB No. 0704-0188

1. AGENCY USE ONLY *(Leave blank)*	2. REPORT DATE	3. REPORT TYPE AND DATES COVERED
	March 1992	Final

4. TITLE AND SUBTITLE

A NOTE ON THE BLAST SIGNATURE OF A CANNON

5. FUNDING NUMBERS

AMCMS No. 6111.02.H610.0
PRON No. 1A13Z1CANMBJ

6. AUTHOR(S)

G.C. Carofano

7. PERFORMING ORGANIZATION NAME(S) AND ADDRESS(ES)

U.S. Army ARDEC
Benet Laboratories, SMCAR-CCB-TL
Watervliet, NY 12189-4050

8. PERFORMING ORGANIZATION REPORT NUMBER

ARCCB-TR-92014

9. SPONSORING/MONITORING AGENCY NAME(S) AND ADDRESS(ES)

U.S. Army ARDEC
Close Combat Armaments Center
Picatinny Arsenal, NJ 07806-5000

10. SPONSORING/MONITORING AGENCY REPORT NUMBER

11. SUPPLEMENTARY NOTES

Presented at the 1992 Joint Army-Navy-NASA-Air Force Propulsion Meeting, Indianapolis, IN, 24-28 February 1992 and published in the Proceedings of the Conference

12a. DISTRIBUTION/AVAILABILITY STATEMENT

Approved for public release; distribution unlimited

12b. DISTRIBUTION CODE

13. ABSTRACT *(Maximum 200 words)*

In a recent experiment with a small caliber cannon, it was found that the early portion of the blast signature was predicted quite well by an inviscid code, but at later times, a secondary shock appeared upstream that was not present in the experiment. The wave is generated as the plume shear layer curls up to form the vortex just downstream of the shock bottle. The second-order solver captures the shear layer more as a slip surface, and the gas stream passing through it retains too much kinetic energy. The shock brings the stream into mechanical equilibrium with the gas ahead of it by converting the excess energy into internal energy. Using a more dissipative solver in the shear layer reduces the kinetic energy of the stream and the shock strength upstream. It is concluded that a practical limit exists for an inviscid calculation of muzzle blast beyond which more realistic dissipative mechanisms must be introduced.

14. SUBJECT TERMS

Muzzle Blast, Blast Simulation, Cannon Blast Flow Field

15. NUMBER OF PAGES

12

16. PRICE CODE

17. SECURITY CLASSIFICATION OF REPORT	18. SECURITY CLASSIFICATION OF THIS PAGE	19. SECURITY CLASSIFICATION OF ABSTRACT	20. LIMITATION OF ABSTRACT
UNCLASSIFIED	UNCLASSIFIED	UNCLASSIFIED	UL

TABLE OF CONTENTS

Page

ACKNOWLEDGEMENTS....ii

INTRODUCTION....1

THE BLAST MODEL....1

RESULTS....1

DISCUSSION....3

CONCLUSIONS....4

REFERENCES....5

TABLES

I. STARTING DATA FOR THE SOLUTION....1

LIST OF ILLUSTRATIONS

1. Surface plots of the pressure and density fields....6
2. Velocity vectors at 0.473 msec....7
3. Shadowgraph of the flow field....7
4. Density plots obtained with second-order solver showing formation of secondary wave....8
5. Velocity vectors for density plot in Figure 4c....8
6. Pressure time histories: (a) experimental data; (b) second-order solver used everywhere; (c) first-order solver used in the shear layer....9
7. Density plots obtained using first-order solver in shear layer....10
8. Velocity vectors for density plot in Figure 7c....10

ACKNOWLEDGEMENTS

The author would like to thank Mr. Doug Savick of Ballistic Research Laboratory for conducting the experiment; Mr. Mick Cipollo of Benet Laboratories for help with the graphics; and LTC Robert E. Dillon of West Point Military Academy for supplying the shadowgraph.

INTRODUCTION

In a recent laboratory study of muzzle blast produced by a cannon (ref 1), it was found that the early portion of the blast signature was predicted quite well by an inviscid code. However, at later times, a secondary wave appeared upstream that was not present in the experiment. In this report, the experimental and numerical data are compared to determine how long the solution remains valid. The source of the wave is identified, and an explanation for its appearance is offered.

THE BLAST MODEL

Harten's scheme (ref 2) is used with a time-splitting algorithm (ref 3) to solve the unsteady axisymmetric Euler equations using the Abel equation of state. A species equation is added to handle the different properties of propellant gas and air. The projectile equation of motion is included.

A uniform grid is used 50 calibers upstream and downstream from the muzzle and 60 calibers radially outward from the axis. Beyond this region, a gradually expanding grid is employed to limit memory while permitting the calculation to continue. Four cells span the tube radius.

As the projectile accelerates in the tube, a shock forms ahead of it. The moving air column is called the precursor flow and is included because it disturbs the quiescent environment prior to projectile exit. The flow behind the projectile is calculated from the Pidduck-Kent limiting solution for an Abel gas (refs 4,5) when its base reaches the position listed in Table I.

TABLE I. STARTING DATA FOR THE SOLUTION

Projectile base position, cm (in.)	143.0 (56.3)
Projectile velocity, m/sec (ft/sec)	1045.0 (3428.5)
Projectile base pressure, atm	287.0
Propellant mass, gm (oz)	38.9 (1.37)
Projectile mass, gm (oz)	98.0 (3.47)
Bore diameter, cm (in.)	2.0 (0.787)
Gun chamber volume, cm^3($in.^3$)	41.7
Specific heat ratio	1.25
Molecular weight	22.8
Covolume, cm^3/kg ($in.^3$/lbm)	982.0 (27.2)

The base pressure and projectile velocity are known at this instant from earlier experiments (ref 6). In this manner, the information relating to the combustion, friction, and heat transfer processes is included in the starting data. Prior to this time, analytical expressions for the projectile velocity and position are used to drive the precursor flow. The results presented next were obtained with a 12-caliber extension attached to the barrel to make them consistent with those in Reference 1.

RESULTS

Surface plots of the pressure and density fields are shown in Figure 1. The planar surface surrounding the disturbance is atmospheric pressure. The tube and projectile are drawn with a 'height' of one atmosphere. The maximum pressure plotted was four atmospheres, which accounts for the flat spot just downstream of the muzzle. The spike at the right is due partly to the bluntness of the projectile in the model. The asterisks indicate some of the pressure transducer locations in the experiment. Seven transducers were placed at angles of 15, 30, 60, 90, 120, 150, and 165 degrees with respect to the line of fire, along an arc 30 calibers from the muzzle.

A velocity plot showing every fourth vector is given in Figure 2. The plume boundary at this instant is indicated by the heavy line. The small circles at the right are the gages at the 15- and 30-degree locations.

A shadowgraph of the flow field is shown in Figure 3. The semicircular objects in the upper right-hand corner are the pressure transducer fixtures at the 30- and 60-degree locations. Also visible are the circular striations of the large Fresnel lens used in the optical setup. The photo, taken in an earlier study (ref 6), did not employ the extension used here. However, the added projectile travel has only a modest effect on the flow field and does not diminish the value of the photo for the present discussion.

In the surface plots in Figure 1, the flow upstream consists of the weak precursor shock 'ps' and the main blast wave 'mb', both of which are followed by mild expansions. The 'shock bottle', which extends from the muzzle exit to the Mach disk 'md' and is enclosed by the barrel shock 'bs', contains the strong muzzle expansion 'me'. The highest and lowest pressures in the exterior flow are found in this small region. The reflected shock 'rs' lies just above the triple point 'tp'. The positions of these structures in the shadowgraph are reproduced quite well by the model.

The presence of the projectile produces some interesting perturbations in the flow field near the line of fire. For example, the pressure jump across the main blast wave is a maximum just above the point where it intersects the projectile bow shock 'pbs'. Below this point, the resistance offered by the atmosphere is diminished because of the motion induced in it by the bow shock. As a result, the pressure falls to the level prevailing in the projectile wake where the gas moves at higher velocities.

In the velocity plot, note that the plume at this instant extends to the projectile. When the projectile emerges from the tube, the propellant gas initially expands around it and moves about halfway down the projectile body. Away from the axis, the plume is decelerated by the inertia of the atmosphere, but near the axis, the projectile continually sets the air ahead of it into motion, and the plume makes further progress downstream. When the projectile leaves the plume, a layer of propellant gas expands into its wake because the gas at its base moves at the projectile velocity. The layer appears as a channel along the axis in the density plot and is faintly visible in the shadowgraph. Eventually, it mixes with the surrounding air.

In the density plot of Figure 1, a thickening 'th' of the plume boundary 'pb' occurs about halfway between the muzzle and the Mach disk. This also occurs in the shadowgraph. The velocity plot reveals a small recirculation zone that is actually the initial stage in the development of the vortex. The gas stream inside the plume boundary remains supersonic after being processed by the weak barrel and reflected shocks. A strong secondary shock 'ss' brings the stream into mechanical equilibrium with the slower moving air behind the main blast wave. The shock appears in the shadowgraph, just downstream from the triple point, and extends radially outward to coalesce with the main blast wave.

The density plots in Figure 4 show the continuation of the vortex formation process. Part of the secondary shock diffracts around the front of the plume and travels downstream to overtake the main blast wave. In response to the slower moving air behind the main blast wave, the shock and the supersonic stream follow a counter-clockwise path upstream, as shown in the velocity plot in Figure 5. Upon reaching the plume boundary, the shock increases the pressure on the downstream side of the barrel shock, causing a contraction of the shock bottle, then travels upstream to undergo a Mach reflection off the tube. The stream curls up into the vortex. Shadowgraphs of these events are not available, therefore, the pressure histories will have to suffice to confirm what part of this scenario is real.

The experimental pressure histories are shown in Figure 6a. The computed histories for the flow described above are shown in Figure 6b. The Fresnel lens used in the optical setup was removed when the histories were recorded to avoid reflecting the main blast wave back into the flow field. Zero time corresponds to the instant the projectile base leaves the barrel.

At the upstream locations, the traces start with the arrival of the weak precursor shock 'ps', as indicated at the top of Figure 6. This is followed by the main blast wave 'mb' and an expansion wave 'ew' that reduces the pressure to sub-atmospheric levels. Forward of the muzzle, the main blast wave overtakes the precursor shock before the gages are reached, as shown in the surface plots. The arrival times and early portions of the computed traces show satisfactory agreement with the experiment.

The secondary shock 'ss' arrives at the 30-degree location first (Figure 4b), the 15- and 60-degree locations next (Figure 4c), then the 90-degree location (Figure 4d). The experimental and computed histories show satisfactory agreement up to this point in time, as indicated by the letters 'ss' in Figure 6. At later times, however, the computed shock undergoes a Mach reflection at the tube surface, which accounts for its strength at the upstream locations. Nothing of comparable strength appears in the experimental traces. An explanation is offered in the next section.

DISCUSSION

The solution was obtained with a second-order solver designed to capture shocks and contact surfaces. However, the blast problem also contains slip surfaces. Consider the velocity plot in Figure 5. One slip surface separates the high speed plume flow from the slower moving air at the plume boundary. A second slip surface develops in the plume interior, downstream of the triple point, and separates the high velocity stream processed by the reflected shock from the slower moving gas processed by the Mach disk. In an inviscid flow, the tangential velocity component and density are discontinuous across a slip surface. The model tries to replicate this, but the surface is smeared by 'numerical viscosity' and, more importantly, the distributions of velocity and density are incorrectly predicted. The high velocity gas stream retains too much kinetic energy as it moves through the flow field, and a strong secondary shock is needed to bring the stream into mechanical equilibrium with the surrounding flow. In the laboratory, dissipative processes at the stream boundaries convert the excess energy to internal energy before the secondary shock is reached.

This explanation can be tested very simply. Knowing that first-order solvers are more dissipative at contact surfaces, a second solution was obtained with the calculation in the neighborhood of the high velocity stream limited to this order. The solution was started with the data in Figure 1 where the stream can easily be identified. The results are shown in the density and velocity plots of Figures 7 and 8. The added dissipation produces a more lethargic stream that curls up earlier to form the vortex and a secondary shock that is weaker everywhere, as indicated by the pressure histories in Figure 6c. The flow in the laboratory lies somewhere between the two solutions. To obtain closer agreement, dissipation must be added more realistically, for example, by solving the Navier-Stokes equations with a turbulence model, at least within the plume. The boundary layer in the tube may also represent an important source of vorticity in the shear layer. Finer grids and increased cpu time are implied.

A related study was made by Cooke and Fansler (ref 7) where the muzzle flow exhausted into a cylindrical muffler. The calculated pressure histories contained oscillations that were not present in the experiment. Identifying their source was difficult because the flow includes reflected waves. The authors suggested that a more realistic treatment of the shear layer might be required, and the present discussion would appear to support their view.

The fascinating transient inviscid flow studies of extragalactic jets made by Norman, Smarr, Winkler and Smith (ref 8) are computationally related. Although the jet-to-ambient pressure ratio of the blast problem is higher by two orders of magnitude, the dynamics and structures are quite similar.

CONCLUSIONS

The early portion of the blast signature is predicted satisfactorily because the flow following projectile exit is inertia-dominated. However, as the flow develops, dissipation in the shear layer becomes important, and a more realistic model is needed to properly account for its effects. While this represents a practical limit to an inviscid calculation near the muzzle, the solution farther away remains valid until the secondary wave arrives. In Reference 1, the model showed good agreement with experimental data out to 50 calibers, including cases where a muzzle brake was used.

REFERENCES

1. Carofano, G.C., "Blast Field Contouring Using Upstream Venting," Benet Laboratories Technical Report in publication.

2. Harten, A., "High Resolution Schemes for Hyperbolic Conservation Laws," J. Computational Physics, Vol. 49, 1983, p. 357.

3. Carofano, G.C., "Blast Computation Using Harten's Total Variation Diminishing Scheme," ARLCB-TR-84029, Benet Weapons Laboratory, Watervliet, NY, October 1984.

4. Carofano, G.C., "The Gasdynamics of Perforated Muzzle Brakes," ARCCB-TR-88006, Benet Laboratories, Watervliet, NY, February 1988.

5. Corner, J., Theory of the Interior Ballistics of Guns, John Wiley and Sons, NY, 1950.

6. Dillon, R.E. Jr., "A Parametric Study of Perforated Muzzle Brakes," ARLCB-TR-84015, Benet Weapons Laboratory, Watervliet, NY, May 1984.

7. Cooke, C.H. and Fansler, K.S., "Numerical Simulation and Modeling of a Muffler," BRL-MR-3735, Ballistic Research Laboratory, Aberdeen Proving Ground, MD, January 1989.

8. Norman, M.L., Smarr, L., Winkler, K.-H.A., and Smith, M.D., "Structure and Dynamics of Supersonic Jets," Astronomy and Astrophysics, Vol. 113, 1982, p. 285.

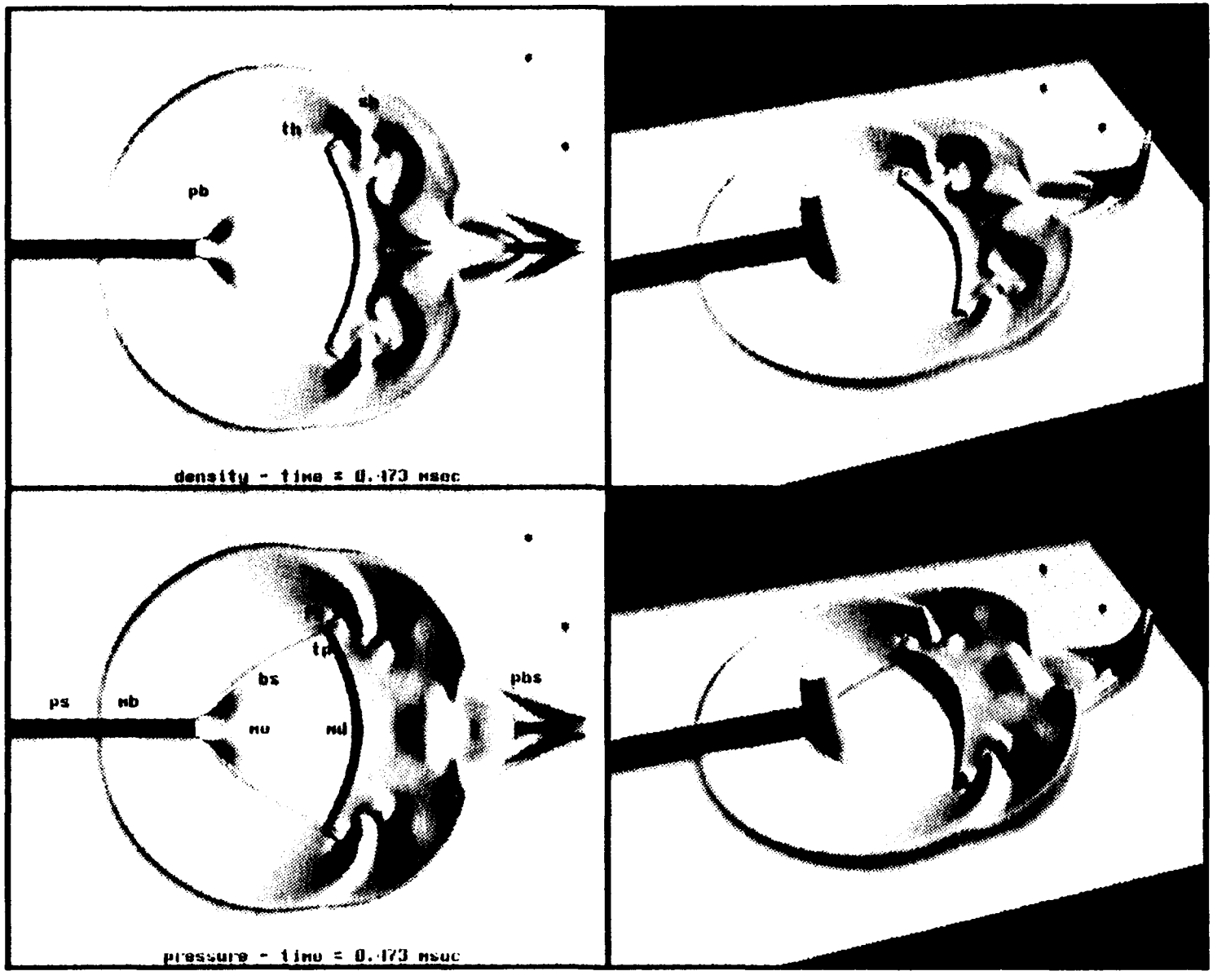

Figure 1. Surface plots of the pressure and density fields.

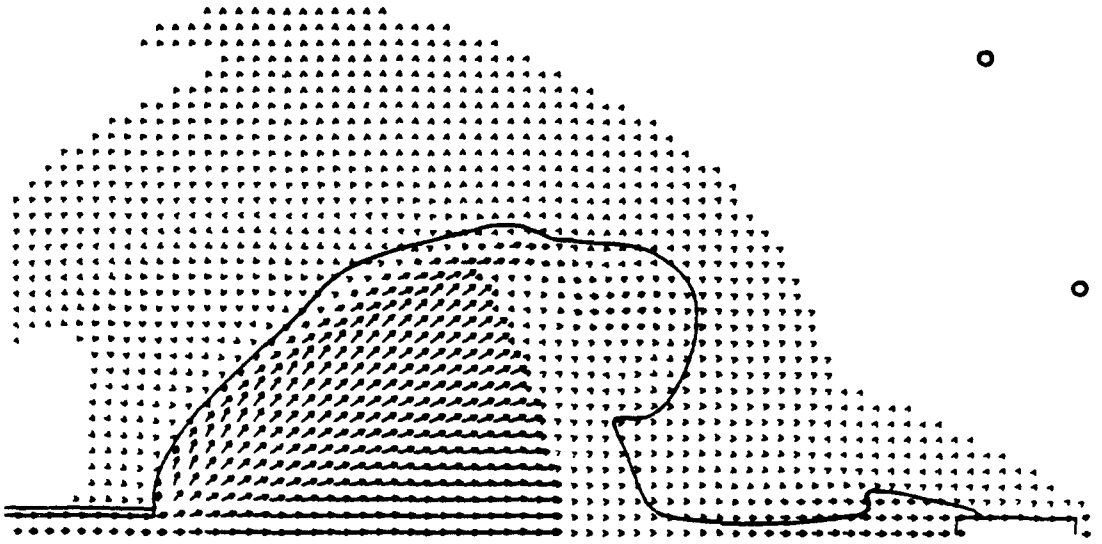

Figure 2. Velocity vectors at 0.473 msec. Contour plot of the mass fraction of the propellant gas with the contours tightly spaced around the level 0.25.

Figure 3. Shadowgraph of the flow field.

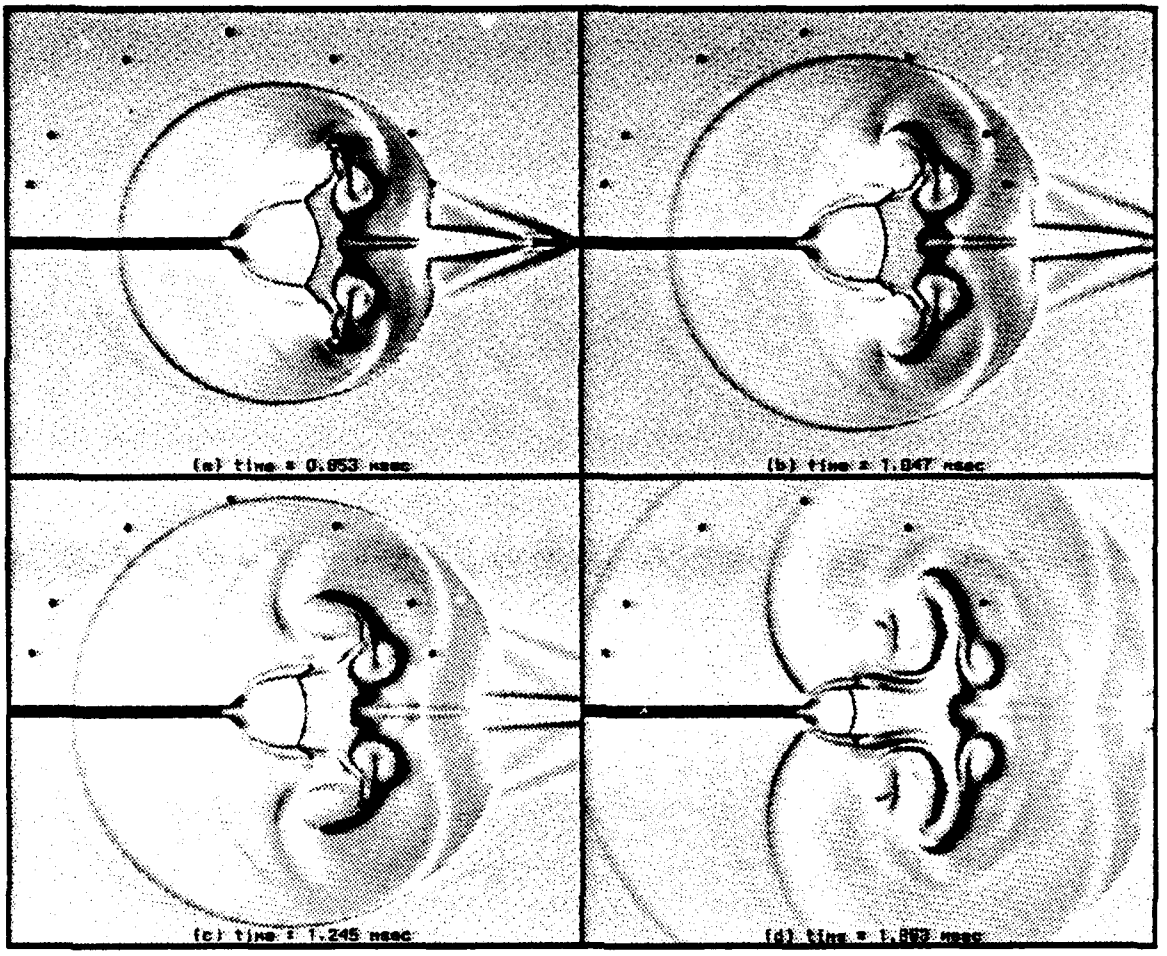

Figure 4. Density plots obtained with second-order solver showing formation of secondary wave.

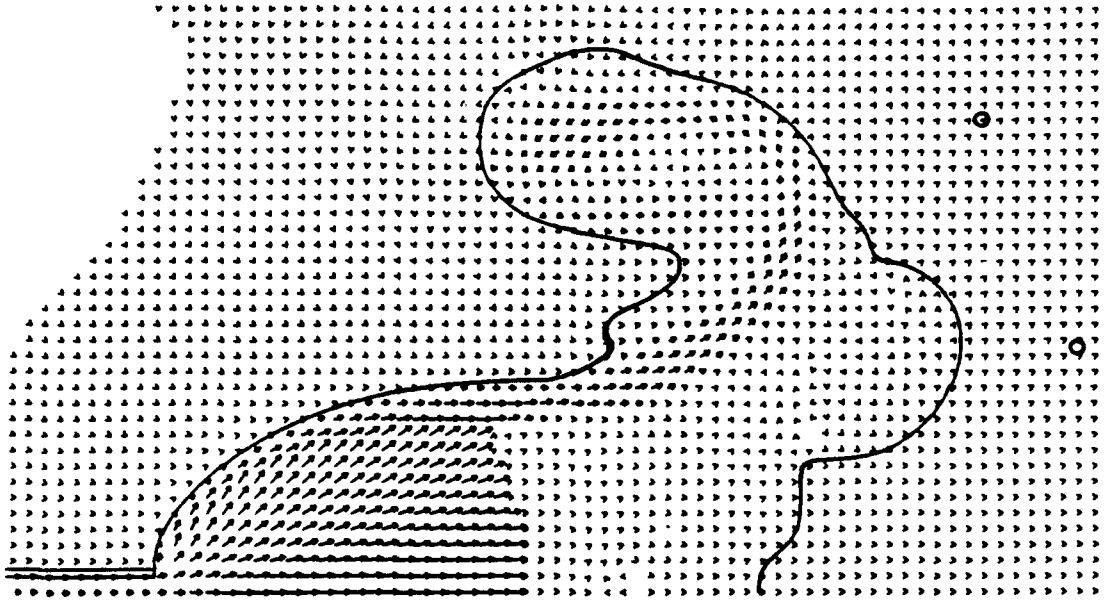

Figure 5. Velocity vectors for density plot in Figure 4c.

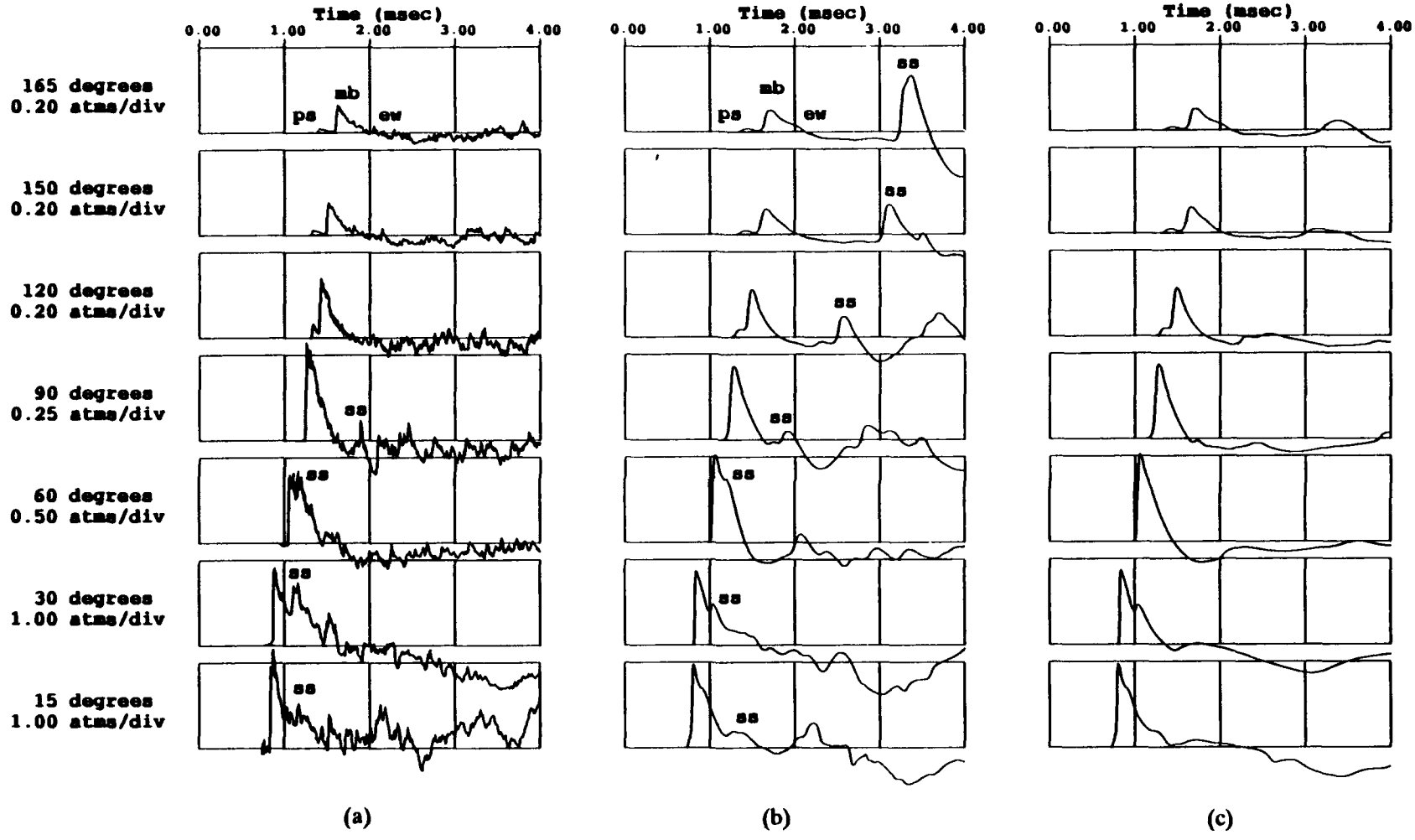

Figure 6. Pressure-time histories: (a) experimental data; (b) second-order solver used everywhere; (c) first-order solver used in the shear layer. The ordinate of each sub-grid represents overpressure (pressure above atmospheric pressure) measured in atmospheres.

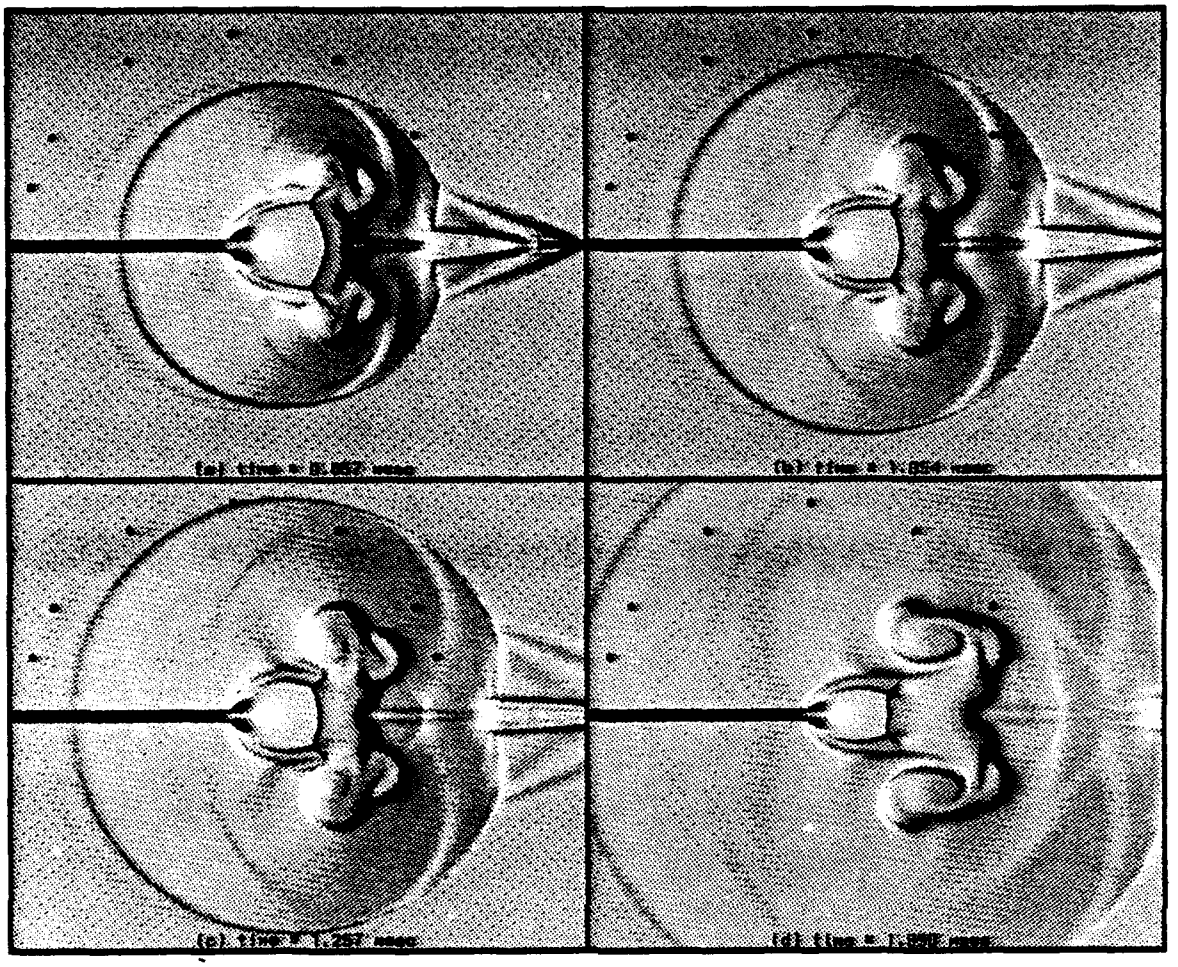

Figure 7. Density plots obtained using first-order solver in shear layer. Note weaker secondary wave.

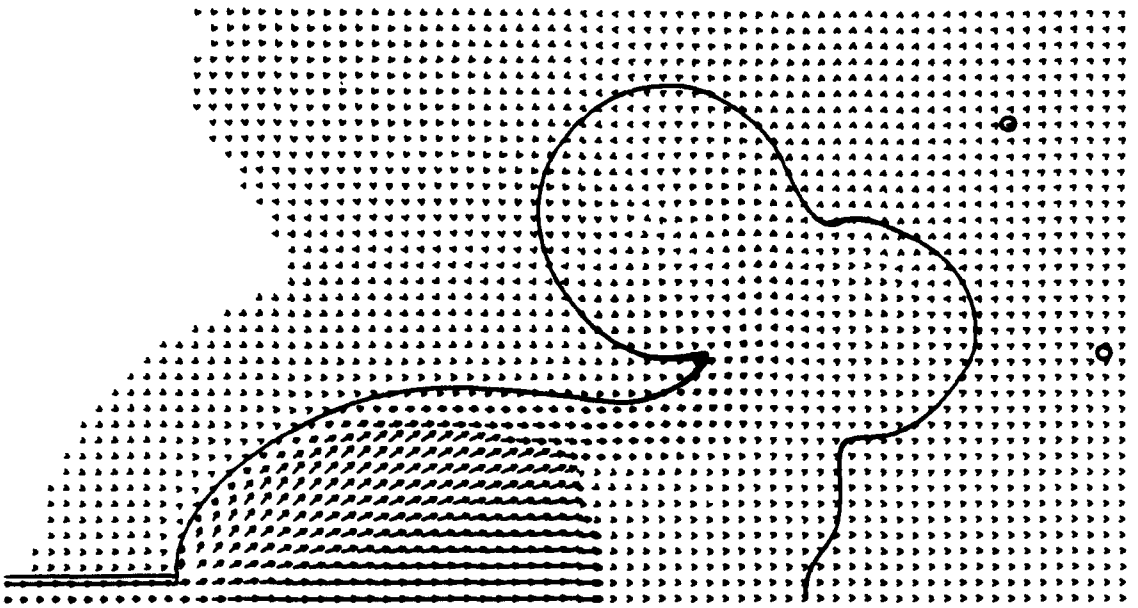

Figure 8. Velocity vectors for density plot in Figure 7c.

TECHNICAL REPORT INTERNAL DISTRIBUTION LIST

	NO. OF COPIES
CHIEF, DEVELOPMENT ENGINEERING DIVISION	
ATTN: SMCAR-CCB-DA	1
-DC	1
-DI	1
-DR	1
-DS (SYSTEMS)	1
CHIEF, ENGINEERING SUPPORT DIVISION	
ATTN: SMCAR-CCB-S	1
-SD	1
-SE	1
CHIEF, RESEARCH DIVISION	
ATTN: SMCAR-CCB-R	2
-RA	1
-RE	1
-RM	1
-RP	1
-RT	1
TECHNICAL LIBRARY	5
ATTN: SMCAR-CCB-TL	
TECHNICAL PUBLICATIONS & EDITING SECTION	3
ATTN: SMCAR-CCB-TL	
OPERATIONS DIRECTORATE	1
ATTN: SMCWV-ODP-P	
DIRECTOR, PROCUREMENT DIRECTORATE	1
ATTN: SMCWV-PP	
DIRECTOR, PRODUCT ASSURANCE DIRECTORATE	1
ATTN: SMCWV-QA	

NOTE: PLEASE NOTIFY DIRECTOR, BENET LABORATORIES, ATTN: SMCAR-CCB-TL, OF ANY ADDRESS CHANGES.

TECHNICAL REPORT EXTERNAL DISTRIBUTION LIST

	NO. OF COPIES
ASST SEC OF THE ARMY RESEARCH AND DEVELOPMENT ATTN: DEPT FOR SCI AND TECH THE PENTAGON WASHINGTON, D.C. 20310-0103	1
ADMINISTRATOR DEFENSE TECHNICAL INFO CENTER ATTN: DTIC-FDAC CAMERON STATION ALEXANDRIA, VA 22304-6145	12
COMMANDER US ARMY ARDEC	
ATTN: SMCAR-AEE	1
SMCAR-AES, BLDG. 321	1
SMCAR-AET-O, BLDG. 351N	1
SMCAR-CC	1
SMCAR-CCP-A	1
SMCAR-FSA	1
SMCAR-FSM-E	1
SMCAR-FSS-D, BLDG. 94	1
SMCAR-IMI-I (STINFO) BLDG. 59	2
PICATINNY ARSENAL, NJ 07806-5000	
DIRECTOR US ARMY BALLISTIC RESEARCH LABORATORY ATTN: SLCBR-DD-T, BLDG. 305 ABERDEEN PROVING GROUND, MD 21005-5066	1
DIRECTOR US ARMY MATERIEL SYSTEMS ANALYSIS ACTV ATTN: AMXSY-MP ABERDEEN PROVING GROUND, MD 21005-5071	1
COMMANDER HQ, AMCCOM ATTN: AMSMC-IMP-L ROCK ISLAND, IL 61299-6000	1
COMMANDER ROCK ISLAND ARSENAL ATTN: SMCRI-ENM ROCK ISLAND, IL 61299-5000	1
DIRECTOR US ARMY INDUSTRIAL BASE ENGR ACTV ATTN: AMXIB-P ROCK ISLAND, IL 61299-7260	1
COMMANDER US ARMY TANK-AUTMV R&D COMMAND ATTN: AMSTA-DDL (TECH LIB) WARREN, MI 48397-5000	1
COMMANDER US MILITARY ACADEMY ATTN: DEPARTMENT OF MECHANICS WEST POINT, NY 10996-1792	1
US ARMY MISSILE COMMAND REDSTONE SCIENTIFIC INFO CTR ATTN: DOCUMENTS SECT, BLDG. 4484 REDSTONE ARSENAL, AL 35898-5241	2
COMMANDER US ARMY FGN SCIENCE AND TECH CTR ATTN: DRXST-SD 220 7TH STREET, N.E. CHARLOTTESVILLE, VA 22901	1
COMMANDER US ARMY LABCOM MATERIALS TECHNOLOGY LAB ATTN: SLCMT-IML (TECH LIB) WATERTOWN, MA 02172-0001	2

NOTE: PLEASE NOTIFY COMMANDER, ARMAMENT RESEARCH, DEVELOPMENT, AND ENGINEERING CENTER, US ARMY AMCCOM, ATTN: BENET LABORATORIES, SMCAR-CCB-TL, WATERVLIET, NY 12189-4050, OF ANY ADDRESS CHANGES.

TECHNICAL REPORT EXTERNAL DISTRIBUTION LIST (CONT'D)

	NO. OF COPIES
COMMANDER US ARMY LABCOM, ISA ATTN: SLCIS-IM-TL 2800 POWDER MILL ROAD ADELPHI, MD 20783-1145	1
COMMANDER US ARMY RESEARCH OFFICE ATTN: CHIEF, IPO P.O. BOX 12211 RESEARCH TRIANGLE PARK, NC 27709-2211	1
DIRECTOR US NAVAL RESEARCH LAB ATTN: MATERIALS SCI & TECH DIVISION CODE 26-27 (DOC LIB) WASHINGTON, D.C. 20375	1 1
DIRECTOR US ARMY BALLISTIC RESEARCH LABORATORY ATTN: SLCBR-IB-M (DR. BRUCE BURNS) ABERDEEN PROVING GROUND, MD 21005-5066	1
COMMANDER AIR FORCE ARMAMENT LABORATORY ATTN: AFATL/MN EGLIN AFB, FL 32542-5434	1
COMMANDER AIR FORCE ARMAMENT LABORATORY ATTN: AFATL/MNF EGLIN AFB, FL 32542-5434	1
MIAC/CINDAS PURDUE UNIVERSITY 2595 YEAGER ROAD WEST LAFAYETTE, IN 47905	1

NOTE: PLEASE NOTIFY COMMANDER, ARMAMENT RESEARCH, DEVELOPMENT, AND ENGINEERING CENTER, US ARMY AMCCOM, ATTN: BENET LABORATORIES, SMCAR-CCB-TL, WATERVLIET, NY 12189-4050, OF ANY ADDRESS CHANGES.